CRYSTAL GROWTH & DESIGN

pubs.acs.org/crystal

Article

Seeded Crystal Growth of the Acentric Organic Nonlinear Optical Material Methyl-*p*-Hydroxybenzoate from the Vapor Phase

Published as part of a Crystal Growth and Design virtual special issue Celebrating John N. Sherwood, Pioneer in Organic and Molecular Crystals

Wenbo B. Hou, Radoljub I. Ristic,* John N. Sherwood, and Ranko M. Vrcelj

Cite This: https://doi.org/10.1021/acs.cgd.3c00097

Read Online

ACCESS | Metrics & More | Article Recommendations | Supporting Information

ABSTRACT: Using *in situ* differential interference contrast microscopy (DICM), growth morphology, structure, and step velocities of the vicinal hillocks on {110} and {11$\bar{1}$} faces of MHB crystal seeds growing from the vapor phase have been investigated over a supersaturation (σ) range of ($0.2 < \sigma < 0.6$). Under these conditions of supersaturation, a dislocation induced growth mechanism was identified. *Ex situ* atomic force microscopy (AFM) shows that some dislocation induced hillocks exhibit hollow cores. The general observations of the {110} and {11$\bar{1}$} surfaces reveal that these faces follow a classical mode of layer growth, continuous generation of new layers by dislocation outcrops, which subsequently bunch and spread to cover the entire facets. A tangential step velocity of the slow and fast sides of {110} and {11$\bar{1}$} growth hillocks show a linear dependence with supersaturation in the region of ($0.2 < \sigma < 0.4$). Analysis of this dependence leads to the respective growth parameters for the identified growth mechanism: the activation energies for the slow and fast step motion of a growth hillock (E_{aS} and E_{aF}) and the corresponding kinetic coefficients (β_{aS} and β_{aF}), for both faces. The growth from physical vapor transport (PVT) shows that for the title material, as with a number of other polar materials, solvent poisoning is not the cause of the highly differential growth rates and is an intrinsic feature of the crystal. The results suggest that in terms of the production of large single crystals of high perfection by PVT, the supersaturation range for dislocation growth should be between 0.2 and 0.4. These findings provide a foundation for the rational design of large MHB crystals that may find applications utilizing their high optoelectronic potential.

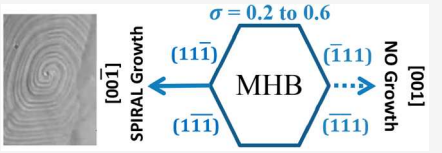

INTRODUCTION

The requirement for highly efficient nonlinear optical (NLO) materials for use in the fabrication of optical switching and amplification devices in the areas of optical processing and communication has led to the investigation of the potential of organic NLO materials for this purpose.[1] To evaluate such materials it is necessary to produce single crystals of high structural and optical perfection, free of strain and defects. When crystals are grown from solution and the melt, solvent and decomposition products in the melt can introduce impurities and imperfection into the as-grown crystals. More problematically, solvent has been reported to cause growth inhibition that limits the sizes of crystals obtainable.[2−4] For crystals grown from the vapor phase, at temperatures below the melting point and in the absence of solvent, this cannot occur and the method promises to yield single crystals of higher quality. It also promises to allow the formation of crystals of materials that cannot be grown from solution due to a persistence of solvate formation[5] with the growth solvent. It could also allow the preparation of polymorphic forms only stable in areas inaccessible to other techniques.

Physical vapor transport (PVT) has been used extensively for preparation of group III/IV and II/VI inorganic semiconductor compounds for electro-optical applications and has proved to be very successful.[6−8] Despite the considerable active development in the inorganic area, relatively little attention has been paid to parallel methods for the growth of organic NLO materials. Whereas sublimation has been for some time a well-recognized technique for the purification of organic materials, it was not until the 1930s that Volmer and Schultze[9] investigated the potential of the method for crystal growth. This early work was later followed by others such as Bradley and Dury,[10] Honigmann and co-workers,[11,12] and Dunning and co-workers.[13−15] The principal purpose of these studies was to examine the kinetics of vapor phase growth in order to test current theories of crystal growth. It was not directed to crystal production. Early attempts at scale-up commenced in the late 1960s, and the equipment used can be classified into two types; (a) controlled self-nucleation on the wall of a static vessel (Sloan,[16] Karl[17]) and (b) self-nucleation at the tip of a moving vessel.[18]

Received: January 30, 2023
Revised: May 18, 2023

Despite the proven applicability of vapor phase growth to the preparation of organic crystals, the method has been little used for highly polar nonlinear optical (NLO) crystals. The only organic NLO crystal for which growth by PVT has been attempted is urea. Feigelson et al.[19] developed a "semiopen" vapor growth system to grow urea crystals in sizes up to about 1 cm, sometimes with well-defined faceting. X-ray topographic examination of the as-grown crystal revealed only striations in the sample. No other defect details, such as dislocations, growth sector boundaries, and inclusions could be resolved. Subsequent improvements to the technique by Zha et al.[20] led to the definition of conditions for improvement of the product crystals by counteracting the reaction of urea to form a biuret, a known habit modifier. Their work showed the potential of the technique for yielding very high-quality crystals. Neither study attempted to define the best supersaturation regime for perfect growth.

There is a need to examine the general problems of the wider applications of the technique and the fundamental influence of the kinetics and mechanisms of growth on crystal production. In this series of papers[21−23] we report the growth of crystals of methyl-*p*-hydroxybenzoate (MHB) by PVT methods as a study in the growth of highly polar organic NLO materials using both self-nucleation and seeded techniques. This manuscript is directed to the better understanding of the technical background to seeded growth.

MHB (Figure 1) has been identified as a promising nonlinear optical material. The second harmonic generation

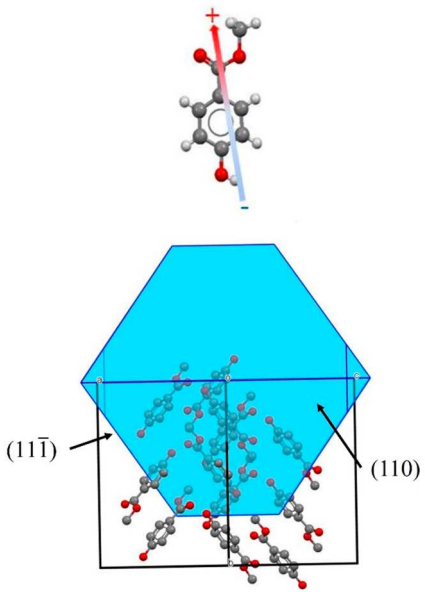

Figure 1. (a) The molecular structure of MHB showing the orientation and sign of the molecular dipole. (b) The crystallographic structure of MHB as viewed perpendicular to the (101) plane superimposed on the Bravais-Friedel-Donnay-Harker (BFDH) prediction of the morphology of MHB. (110) and (11$\bar{1}$) faces are indicated. Note that morphology calculation programs do not differentiate between the absolute polar directions.

efficiency of powder samples was first reported by Jerephagnon.[24] A number of other publications of both its crystal growth from solution and its optical performance have followed which confirmed its optical potential. The fundamental reason MHB can fulfill this optical potential is because it has an acentric crystallographic structure. This raises some intriguing questions on its crystal growth properties.

Following studies of the growth from solution of the acentric material α-resorcinol Wells[2−4] found that crystals of this material grew only in one polar direction. Later assessments of this and related materials confirmed that this property was also held by a wide range of other highly polar acentric organic crystals. Wells concluded that this property was a consequence of the differential adsorption of solvent on the positive and negative ends of the polar crystals. From the viewpoint of the crystal grower this places a limit on the production of crystals: only half crystals can be grown. In an effort to overcome this limitation Sherwood and Srinivasan[25] proposed that the problem could be solved by growth from the vapor phase. α-Resorcinol crystals grown from the vapor phase however showed the same unidirectional growth.

Despite the numerous studies of the growth of MHB this behavior has never been recognized for this material. Our recent study[21] shows that this material does exhibit this property. It has not been recognized previously for the simple reason that the half crystals previously produced have been adequate for the purpose that they were grown. The present examination provides further absolute evidence of its existence and takes the definition of the effect to a new level. It poses questions on the long-held interpretation of Wells[2−4] results by implying that solvent/surface interactions have little or no significant surface effect on crystal growth and hence morphology.

In a preceding publication[21] we have developed an understanding of the preparation of small crystals ($\lesssim$1 cm^3) of this material as single crystals by self-nucleation PVT. Two principal factors emerged from this study. Growth of crystals in the supersaturation region ascribable to dislocation-controlled growth led to the best product. Progress to supersaturations higher than those for dislocation growth led to the additional onset of 2D nucleation-type mechanisms prone to the incorporation of unwanted impurities and structural inhomogeneities into the crystal lattice. Since the growth of larger crystals is usually achieved using seeded growth under more controllable conditions the results of the present study are thus essential for the definition of these conditions and hence for the controlled growth of crystals by the seeded PVT process.

In this paper, we investigate the PVT growth behavior of seeded MHB crystals growing by dislocation growth mechanism and define the true growth supersaturation range, in which the large single crystals could be prepared with as high an optically and structurally perfect form as is possible. For this purpose, we consider the growth of {110} and {11$\bar{1}$} faces because they form the major growth sectors in the crystal and hence make a major contribution to the volume of usable material following growth. In order to control the physical properties of this crystal, with respect to both crystal structure perfection and optical properties, it is crucial to appreciate the growth processes, in real time, on the micrometer- and nanometer-scale morphology of the crystalline surfaces. With this in mind, we report *in situ* differential interference contrast microscopy (DICM) and *ex situ* atomic force microscopy (AFM) measurements of the {110} and {11$\bar{1}$} faces over a supersaturation range in which a dislocation induced growth mechanism operates. We investigate morphology and dislocation structure of the respective vicinal growth hillocks of the two faces with a variation of external growth conditions of supersaturation and temperature as well as the bunching of the

https://doi.org/10.1021/acs.cgd.3c00097
Cryst. Growth Des. XXXX, XXX, XXX−XXX

dislocation generated steps. We also report on the anisotropic step velocities along the slow and fast side of the {110} and {11$\bar{1}$} growth hillocks over the established range of supersaturation and estimate the growth parameters, for the slow and fast step motion of a growth hillock (E_{aS} and E_{aF}) and the corresponding kinetic coefficients (β_{aS} and β_{aF}), for the respective faces. In conclusion, the main results of the paper are summarized and critically discussed.

EXPERIMENTAL SECTION

Materials, Purification, and Structure. Details of the purification and purity of the materials used in these experiments have been given in the first part of this series of papers together with all structural information regarding the acentric nature of MHB.[21] A few appropriate points are repeated here that are relevant to this particular aspect of this study.

Saturation Vapor Pressures (SVPs). SVPs for MHB were assessed by extrapolation of the recently published data of Perlovich et al.[26] Using a dynamic assessment technique in the temperature range 30 to 54 °C these authors showed that the SVPs follows a relationship:

$$\ln(p[\mathrm{Pa}]) = (34.3 \pm 0.3) - (11{,}889 \pm 92)/T(K)$$

In the present PVT experiments supersaturations are given as $\sigma = \frac{C_0(T_0) - C(T)}{C_0(T_0)}$, where $C_0(T_0)$ is the estimated concentration corresponding to p_0 of the SVP at the source temperature, T_0, and $C(T)$ that corresponds with p at the deposition temperature, T. Details are given in the attached Supporting Information (SI S1).

The Growth Cell. Full details of the PVT growth cell, its operation, and its performance are given in the SI S2 for this manuscript.

Microscopy. Optical microscopy was carried out *in situ* in the growth cell using a Leitz-Reichart Polyvar 2 microscope. The techniques used in the various optical examinations were differential interference contrast microscopy (DICM) for the general observation of surfaces, growth centers, and the kinetics of growth steps of individual growth hillocks; and two-beam interference microscopy (TBIM) (monochromatic green light: $\lambda \approx 540$ nm) for the assessment of macrostep height. The surface morphological events on the major crystallographic faces were simultaneously monitored and recorded either (i) by a time-lapse photography technique or (ii) by TV video tape recording. The latter was that mainly used. (Details expanded in SI S3.)

These optical techniques were supplemented by *ex situ* atomic force microscopy (AFM) for the more detailed examination of growth centers.

RESULTS AND DISCUSSION

Our previous studies of growth of MHB by self-nucleation[21] confirmed two factors concerning the range of conditions needed to provide information on the best supersaturation range within which to produce crystals of high perfection. These factors are common to the growth of all crystals no matter their size, macro or micro, and whether they are grown by PVT, melt, or solution growth. First, at very low supersaturations little or no growth occurs on all crystal faces.[27,28] As the supersaturation increases growth by dislocation sources initiates and growth commences. This continues for a period, giving way to other layer growth mechanisms and finally to rough growth mechanisms. X-ray topographic studies of grown crystals showed that the best perfection was achieved during the regime of dislocation induced growth with structural imperfection increasing as the other mechanisms come in to play. This is not new information and is an expected progression.[29] However, it guides us in this particular case to our working region. To achieve the "sweet range" for perfect growth requires that we sweep the lower supersaturation range, immediately above the termination of the "dead" range, to identify the area within which to work. We know from our previous experiments on self-nucleation that this will be well below the lowest self-nucleation supersaturation temperature range identified in our previous publication[21] as source temperature 393 K/nucleation temperature 363 K: σ = 0.92. The study was therefore commenced at the lowest supersaturation at which seeded growth could be detected (σ = 0.2). All experiments (other than those reported for AFM microscopy) were carried out *in situ* in the growth cell. Under these conditions the predominant morphology of the crystals was of an octahedral habit with four large {110} faces and, in the negative [00$\bar{1}$] direction, smaller (11$\bar{1}$) and ($\bar{1}$1$\bar{1}$) faces. As shown previously, little or no growth occurred in the positive [001] direction.

Morphology and Dislocation Structure of Growth Hillocks. Growth hillocks on both faces showed a pronounced anisotropy and complex shape associated with the underlying crystallographic structure. Those on the (11$\bar{1}$) faces were aligned with the long axes along [1$\bar{1}$0] (fast growth) and the short axes normal to this direction (slow growth). Those on {110} faces were aligned with long [1$\bar{1}$2] and short [1$\bar{1}$1] directions, fast and slow growth, respectively. Figure 2 confirms

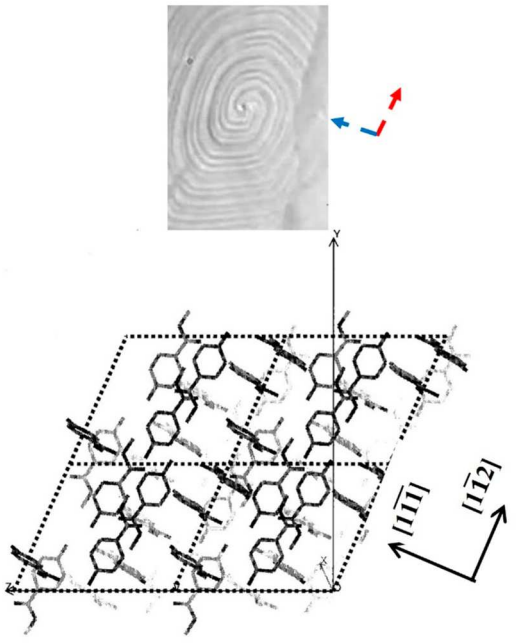

Figure 2. Orientation of a growth hillock on the {110} face of an MHB crystal and its relationship to the underlying crystal structure. Fast growth along [1$\bar{1}$2] (dashed red arrow) and slow growth along [1$\bar{1}$1] directions (dashed blue arrow).

for the latter case that the maximum and minimum molecular interactions lie along these directions. This accounts for the later observed anisotropic step velocities of the terraced hillocks.

As an example of studying a hillock structure and genesis in the grown crystals we consider hillocks on the {11$\bar{1}$} which have common growth features with those on the {110} faces. Figure 3 presents an enlargement of the growth centers on a {11$\bar{1}$} face using *in situ* DICM time-lapse photography. This

https://doi.org/10.1021/acs.cgd.3c00097
Cryst. Growth Des. XXXX, XXX, XXX−XXX

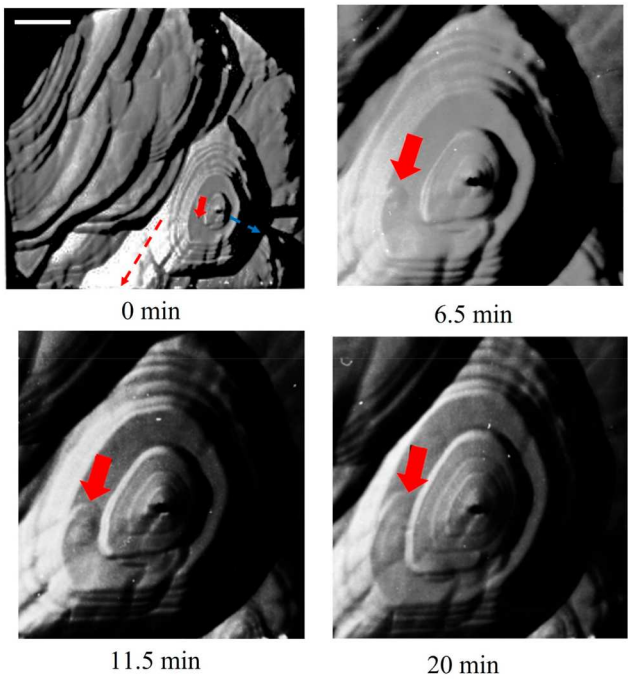

Figure 3. *In situ* DICM images of the resurrection and growth of a buried dislocation source in the indicated area, identified with a thick red arrow, the $\{11\bar{1}\}$ face. Scale bar 20 μm. Dashed red arrow indicates the direction of fast growth; dashed blue arrow indicates the direction of slow growth.

demonstrates not only that the surface of this crystal is covered by overlapping and potentially over-riding growth hillocks but also how they constantly regenerate to maintain a continuing growth rate.

At zero time of observation the flat area adjoining the major growth hillock (arrowed) is featureless. As time progresses a dislocation emerges from below and within 20 min has emitted 3−4 turns of a renewed source. The shape and orientation of this source matches perfectly those of the surrounding active sources. Obviously the initiating dislocation has been overridden at earlier times by other more strongly growing dislocations but has burrowed its way through to resurrect its activity. This is good evidence to show how dislocations can perpetuate unless they are terminated at significant defects in the system.

The figure shows four successive stages of a major spiral and the resurrection of the neighboring dislocation source (arrowed), at successive points in time. Under the same conditions of supersaturation, which must exceed the critical value for the activation of the new source, the arrowed source becomes activated, but its power of growth steps production is considerably smaller than that of the adjacent major source; characterized by the increased number of emitted growth steps in the same time period. This finding implies not only the necessity of providing the level of supersaturation above that critical for resurrection but also the existence of a distinct variation of dislocation activities among the growth hillocks operating at the same facet under the same growth conditions of temperature and supersaturation. This variation is due to the different number and configuration of dislocation outcrops in each growth step source including the amount of strain induced in its center.[29]

This time-dependent set of photos demonstrates unambiguously:

- The activation (resurrection) of the arrowed growth hillock
- The fixed position in space and time of its apex (the outcrop of screw or mixed dislocation(s)) which provides continuous step growth
- The constancy of the spiral shape

Other than the lack of need for the resurrection the same applies to the neighboring, originally nonburied growth hillock of a considerably bigger net Burgers vector (∼activity) of the bunched screw or mixed type dislocation outcrops located at its apex, i.e., the hillock of higher activity would operate at a supersaturation lower than that imposed, while the other hillocks would be inactive.

Further studies expanded our confidence that the region chosen for study was that governed by dislocation induced step-flow type growth mechanism.

Video recording is in principle similar to time-lapse photography, but more inclusive and informative. It enabled the simultaneous monitoring and video recording, in real-time, of the structure and dynamics of dislocation step source of a growth hillock, generation of growth steps, and their consequent spreading and bunching across a face of interest. Several different spiral patterns, originating from complex dislocation sources, have been observed in the range of the imposed external growth conditions of growth temperature T (383 K $\leq T \leq$ 390 K) at constant source temperature T_0 = 393 K (corresponding supersaturation range 0.535 $\geq \sigma \geq$ 0.216). At the point where an isolated single screw or mixed type dislocation outcrop reaches the surface often a single spiral develops. If two dislocation outcrops or a bundle of screw or mixed type dislocations are involved, other spiral forms, such as multiple spirals and Frank Read-type spirals may occur.

Figure 4 shows four snapshots of typical spirals on a (110) face the movements of which were continuously video recorded at four different growth temperatures T or corresponding supersaturations σ. Figure 4a (T = 383 K, σ = 0.535) shows the growth hillock with a short dark line on the top of it. On enlargement, this feature resolves into an array of three active dislocations in a complex step source; Figure 4b (T = 387 K, σ = 0.377) represents two neighboring single spiral sources; Figure 4c (T = 388 K, σ = 0.315), double spiral source; and Figure 4d (T = 390 K, σ = 0.215), two neighboring double spiral sources. A similar pattern of behavior was observed on the $(11\bar{1})$ faces over the same region of supersaturation.

Therefore, the key findings for the spiral step behavior in the region of growth temperature (383 K $\leq T \leq$ 390 K) or in the respective region of supersaturation (0.535 $\geq \sigma \geq$ 0.215) are as follows:

- There is no influence of either temperature or supersaturation on the shape of growth spirals.
- Any of the observed step sources operates as a continuous and topographically fixed dislocation source of spiral steps, regardless of its complexity, suggesting that a dislocation source has an effective (resultant) nonzero screw component of Burgers vector and is being active in terms of the growth steps production at the imposed driving force (supersaturation).
- The growth on nearly the entire (110) face and $(11\bar{1})$ face (Figure 3) occurred on bunched steps (macrosteps)

https://doi.org/10.1021/acs.cgd.3c00097
Cryst. Growth Des. XXXX, XXX, XXX−XXX

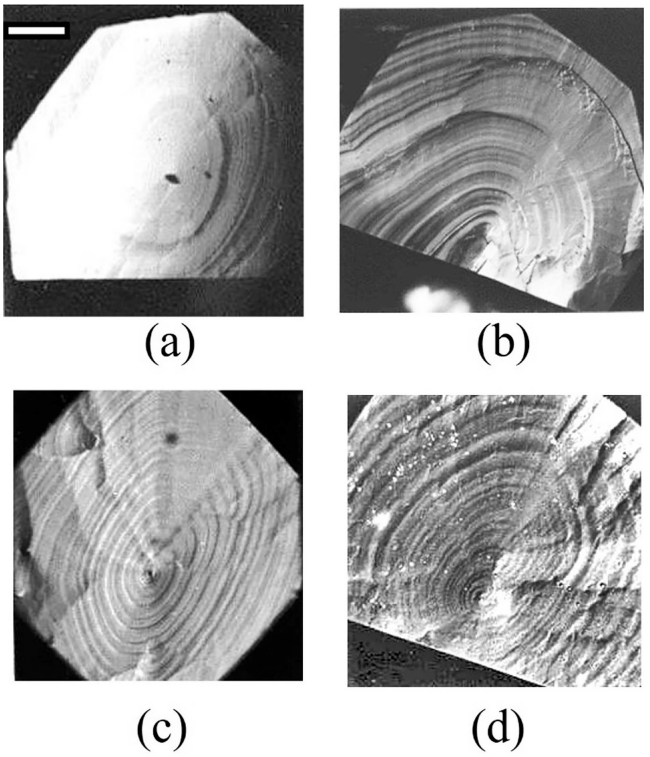

Figure 4. *In situ* DICM images of the growth hillocks on the principal {110} crystal faces as a function of growth supersaturation σ. (a) σ = 0.535, (b) σ = 0.377, (c) σ = 0.315, (d) σ = 0.215. Scale bar 20 μm.

whose terrace width and height, despite some fluctuations, tend to increase with distance from the top of the hillock regardless of σ and the respective value of T. With the applied DICM and TBIM ($\lambda \approx 540$ nm), we estimate that the increasing terrace width range is between ~1 and 10 μm and the corresponding range of increasing height of macrosteps is between ~0.2 and 8 μm.

- No detectable growth in the positive [001] direction for the whole range of supersaturation ($0.535 \geq \sigma \geq 0.215$).

To prove the validity of the above statement, we attach as supplementary evidence a typical example, a TV video recorded movie converted to digital image by A/D converter, of the dynamics of the generation of the co-operating spiral steps at the apex of the growth hillock shown in Figure 4c and their consequent bunching and spreading across the growing surface at fixed external growth conditions of temperature, T = 388 K, and supersaturation, σ = 0.315 (SI video). The movie suggests that growth on the {110} faces occurs on elementary steps that quickly begin to bunch into macrosteps and consequently become optically detectable. Regarding elementary steps, they are too low and closely spaced, below the respective vertical (~30 nm) and lateral (~500 nm) resolution thresholds and, as such, cannot be imaged directly by interference light microscopy techniques.[30]

In the present case, however, some confirmation of the existence and location of the initiation of bunching effect can be obtained by AFM. Detail of the distribution of growth steps around a growth hillock on the {110} surfaces was examined using *ex situ* AFM. Figure 5a shows a hollow core of the radius $r_{hc} \sim 0.2$ μm in the center of the growth hillock. In Figure 5b microsteps of ~100 nm high are emitted from the core A suggesting a relatively high Burgers vector b of the step source. Step bunching B, created by a numerous microsteps C, began at near (~2 μm) from the source and increased with distance from the source.

Hollow dislocation cores have been observed in a number of inorganic crystals[31−35] including epitaxially grown films of GaN,[36] but not in a small molecule organics. A comparison of our observed $r_{hc} \approx 0.2$ μm and $b \approx 0.1$ μm for MHB with those of any of the above inorganics, e.g., for silicon carbide (SiC) $r_{hc} \approx 5$ μm and $b \approx 0.5$ μm, confirm that a stable thermodynamical hollow core may exist if their Burgers vectors are in excess of one unit step height, regardless of the nature of a crystal. Qualitatively, our observations are in accordance with theoretical predictions.[37−39] To get a deeper insight into these observations and check a potential validity of the refined theoretical model,[39] a quantification of the dependence of surface vicinality on supersaturation levels including those bellow the range $0.2 < \sigma < 0.6$ and dislocation structure is needed. The two prerequisites for taking forward this problem are (1) a specially design *in situ* AFM measurements system for the PVT growth of MHB and (2) an accurate determination of elastic constants for this low symmetry (monoclinic) system. At present, these issues remain unchallenged.

Step Bunching. Step bunching is one of the very important findings in the layered growth of MHB crystals by PVT. We observed this phenomenon at any supersaturation level, and at present, it seems unavoidable or intrinsic regardless of external conditions. Broadly, step bunches trap point defects resulting in striations within grown crystals.[40]

Generally, step bunching begins at or near the dislocation source, when a group of steps, due to different supersaturation across the surface, get closer to one another, the steps within the group compete for the supply of growth units and, as a consequence, move more slowly. The rear steps behind this group move still faster to catch up and join the retarded group which leads to an increase of both height and spacing with distance from the hillock top and time. The movie shows that these two spatiotemporal evolutionary characteristic features are not equal for any two randomly chosen neighboring bunches (macrosteps) from the sequence of propagating macrosteps. Since the velocities of the adjacent macrosteps are inversely proportional to their heights, the macrosteps must coalesce, and the average height and spacing of the newly created step increases. This typical evolutionary tendency toward achieving the average maximum of both parameters far from the top of the hillock, at a fixed supersaturation, is clearly demonstrated by the movie and the snapshots in Figure 3 and Figure 4.

Understanding of these issues will likely be a pivotal prerequisite for controlling structural and compositional uniformity during crystallization not only in nonlinear optical crystals but also in pharmaceuticals and proteins. Step bunches are well-known and have been thoroughly studied in vapor growth and epitaxy of inorganics[41,42] but much less of organics. Apart from the above findings on PVT growth of MHB, these studies highlight other important issues that need to be resolved. For example, the initial formation of bunches and trapping point defects even at these relatively early stages of their development resulting in striations within the grown crystals, the morphological stability of straight macrosteps and their likely transition into faceted macrosteps in solution growth. The meandering of the latter ones is a danger of defect

https://doi.org/10.1021/acs.cgd.3c00097
Cryst. Growth Des. XXXX, XXX, XXX−XXX

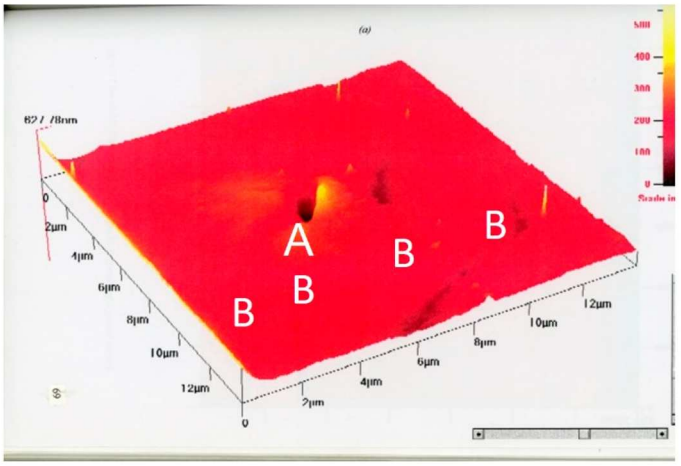

(a)

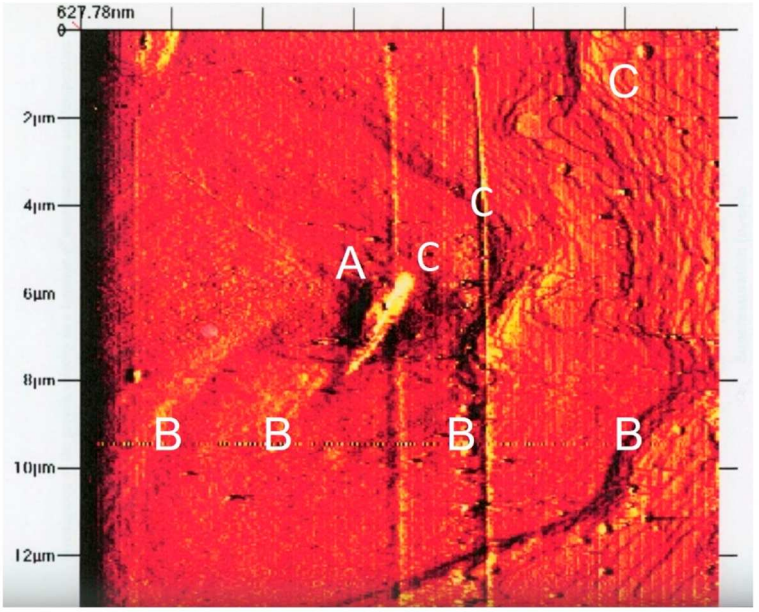

(b)

Figure 5. *Ex situ* typical AFM images at the center of a growth hillock on a {110} face of MHB. A − Dislocation core, B − Macrosteps, C − Microsteps. (a) Perspective view, image size 10 × 10 μm^2. (b) Top-down view, image size 12 × 12 μm^2.

formation like air inclusions. Therefore, if a process of complete removal of the step bunching is unachievable, then an effort of its minimization should be crucial for an additional improvement of high crystal perfection.

Kinetic Studies. These were carried out in the above-defined range of supersaturation with the microscope system operating in DICM mode and by making use of the time-lapse photography technique, illustrated in Figure 3. Therefore, for any of the two faces grown under well-defined condition of supersaturation, the step velocities for two directions, slow and fast, were simply quantified as the ratio of a step displacement obtained from the comparison of their successive photostages and the corresponding time intervals. The kinetic data for both faces are presented in Figure 6 as a function of supersaturation.

{110} Faces. The anisotropic step velocities along the slow and fast side of a {110} hillock of MHB as a function of supersaturation are shown in Figure 6a. In the low supersaturation range (0.2−0.4) these increase initially almost linearly with supersaturation to become almost constant at greater supersaturations. At this stage, we argue that this noticeable step retardation is likely to be caused by a combination of two factors.

First, crystal growth is generally regarded to occur in three steps: (i) volume diffusion of the growth unit from the vapor to the growing surface, (ii) surface diffusion of the growth units to a kink site at a step, and (iii) kink integration. It is well-known that the average distance between the molecules in the vapor phase is 100−1000 times greater than in solution or the melt. Such long distances make it difficult for MHB

https://doi.org/10.1021/acs.cgd.3c00097
Cryst. Growth Des. XXXX, XXX, XXX−XXX

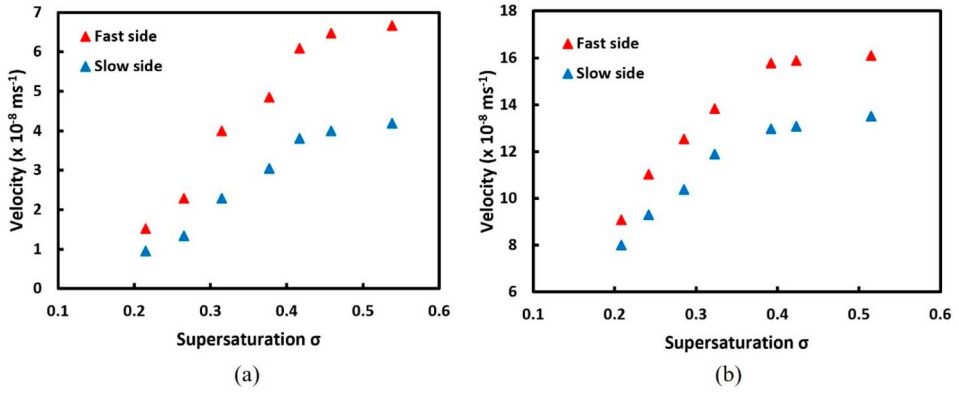

Figure 6. Step velocities vs supersaturation for the fast and slow side of (a) a {110} hillock and (b) a $\{11\bar{1}\}$ hillock.

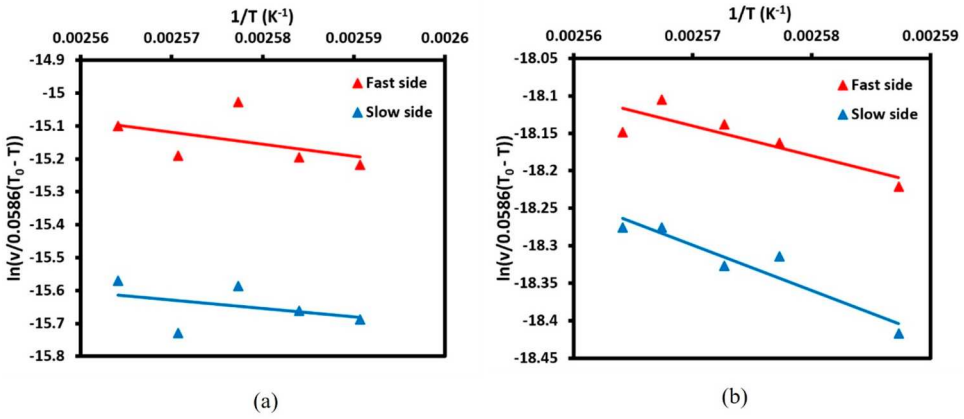

Figure 7. Plot of $\ln(v/0.0586(T_0 - T))$ against $1/T$ for (a) a {110} hillock and $\{11\bar{1}\}$ hillock.

molecules to be adsorbed at the surface compared with the solution and melt growth. Hence the surface energy barrier becomes the highest compared with that for surface diffusion or integration. With an increase of supersaturation and hence molecular concentration in the gas phase, more molecules will be adsorbed and the molecular concentration at the interface will increase. At any specific temperature, the surface diffusion and the average number of kinks in the step will be constant, and the step velocity increases with supersaturation. However, when the supersaturation reaches 0.4 the molecular concentration at the surface becomes saturated, and further increases in the supersaturation will have no effect on the step velocity. Thus, the adsorption of molecules from the vapor phase is the slowest step of the three and determines the growth rate of MHB. Second, hollow cores may also be produced without a spiral by multiple edge dislocation sources as has been observed on SiC.[39,43,44] Generally, a production of hollow cores increases with supersaturation.[44] This suggests that an additional contribution in the growth step deceleration for $\sigma \geq 0.4$ is likely to be caused by the high local stress densities induced by an appreciable increase of a number of edge dislocation hollow cores.

{11$\bar{1}$} Faces. Throughout the study of these faces the growth behavior of the $(11\bar{1})$ and $(1\bar{1}1)$ faces was similar to that of the {110} zone faces. The equivalent measurements are collected in Figure 6b. From the figure we can see that when the supersaturation is lower than 0.4, the step velocities in both directions increase linearly with the increase of supersaturation reaching almost constant value at supersaturations greater than 0.4. This again suggests that under the later conditions the marked change of the growth step deceleration may be a consequence of the two parallel processes occurring on the $(11\bar{1})$ face: (i) the maintenance of the adsorption of molecules from the vapor phase nearly at a saturation level; and (ii) the reduction of tangential step velocities around high density stressed localities generated by newly formed edge dislocations cores.

In summary and with respect to the aim of growing large crystals by seeded growth, the best range of operation is

- Source temperature 393 K
- Growth temperature 390−383 K
- Supersaturation range 0.2−0.4.

Within this range the growth mechanism is dominated by a dislocation induced spiral growth mechanism.

Observation in situ of the movement of growth steps showed that the velocity of step motion in the slow directions was approximately two-thirds of that in the fast direction. Monomolecular steps and macromolecular steps up to 100 nm were observed. It was noted that the height of the steps influenced their velocity and that the lower the steps, the faster they moved. Despite this, it was also found that the step velocity could also vary by up to 100%. No obvious cause could be found for such changes, and we assume that this variation arises from local changes in the supersaturation on the top of the crystal due to concentration or temperature gradients or, alternatively, to free convection in the cell. For individual steps, as time progressed, step pile-ups occurred which also resulted in a gradual slowing of advance. Similar variations have been noted by van Enckevort and co-

https://doi.org/10.1021/acs.cgd.3c00097
Cryst. Growth Des. XXXX, XXX, XXX−XXX

workers[45,46] who reported that the rate of advance of macrosteps was substantially slower than that for the small steps. Generally the step velocities on the (110) and (11$\bar{1}$) faces fall in the range 10^{-7}–10^{-8} ms^{-1} depending on the supersaturation and step height.

Estimation of Kinetic Coefficient and Activation Energy. The activation energy for step motion, E_a, was calculated from an Arrhenius form derived from a step velocity vs temperature and the following formula[47,48]

$$v = \omega\beta(C_0(T_0) - C(T)) \quad (1)$$

where $(C_0(T_0) - C(T))$ can be approximated by $0.001(T_0 - T)$ (for the conversion see Supporting Information S1) where T_0 is the saturation temperature, and β is assumed to be of the form

$$\beta = \beta_0 e^{-E_a/kT} \quad (2)$$

After substitution and unit correction, eq 1 becomes

$$v = 0.0586\beta_0(T_0 - T)e^{-E_a/kT} \quad (3)$$

By taking ln of eq 3 it gives the Arrhenius form

$$\ln\left(\frac{v(T)}{0.0586(T_0 - T)}\right) = -\frac{E_a}{k}\left(\frac{1}{T}\right) + \ln\beta_0 \quad (4)$$

By fitting eq 4 to the linear region of data from Figure 6 (a) and (b), as replotted in Figure 7, values for the activation energies for the slow and fast step motion of a growth hillock (E_{aS} and E_{aF}) and the corresponding kinetic coefficients (β_{0S} and β_{0F}), for the respective (110) and (11$\bar{1}$) faces, were calculated: $E_{aS}^{(110)} \approx 30$ kJ mol^{-1}, $E_{aF}^{(110)} \approx 20$ kJ mol^{-1}, $\beta_{0S}^{(110)} \approx 0.011$ cm s^{-1}, $\beta_{0F}^{(110)} \approx 0.314$ cm s^{-1}, and $E_{aS}^{(11\bar{1})} \approx 50$ kJ mol^{-1}, $E_{aF}^{(11\bar{1})} \approx 33$ kJ mol^{-1}, $\beta_{0S}^{(11\bar{1})} \approx 0.375$ cm s^{-1}, $\beta_{0F}^{(11\bar{1})} \approx 6.26$ cm s^{-1}. These values of E_a and β_0 can be inserted into eq 2 to give corresponding values of β for slow and fast steps of both (110) and (11$\bar{1}$) faces: $\beta_S^{(110)} \approx 1.4 \times 10^{-6}$ cm s^{-1}, $\beta_F^{(110)} \approx 4.7 \times 10^{-4}$ cm s^{-1}, and $\beta_S^{(11\bar{1})} \approx 1.1 \times 10^{-7}$ cm s^{-1}, $\beta_F^{(11\bar{1})} \approx 3.1 \times 10^{-4}$ cm s^{-1}. In spite of fact that MHB are small organic molecules, these values of β are about 4 orders of magnitude smaller than those of typical inorganics such as KH_2PO_4 (KDP)[35] and similar to those of tobacco virus[49] and canavalin[50] polymers. Bearing in mind that the kinetic coefficient itself is a measure of the kinetics of adsorption, diffusion, and incorporation, the potential source for the low value of β in the MHB vapor growth crystals is likely to be a dominant large barrier to adsorption, as discussed in the previous section.

CONCLUSIONS

In situ optical DICM and TBIM techniques have enabled us to quantitatively investigate the spiral growth of the {100} and {11$\bar{1}$} faces of a seeded MHB single crystal growing from the vapor phase, over a supersaturation range of $(0.2 < \sigma < 0.6)$. The techniques allowed, in real time, observations of growth morphology, structure, and step velocities of the growth spirals (hillocks) of the respective faces. Although not studied here, it should be pointed out that faces propagating with a growth vector in the opposite, positive [001] direction, showed little or no growth in the whole range of supersaturation. The morphology of MHB single crystals grown from the vapor phase followed the general pattern of unidirectional growth of the class of structurally acentric solids grown from solution.

Growth hillocks on both {100} and {11$\bar{1}$} faces show a pronounced anisotropy and complex shape associated with the underlying crystallographic structure. We demonstrate not only that the investigated surfaces are covered by overlapping and potentially over-riding growth hillocks but also how they get activated and constantly resurrected to maintain a continuing growth rate, at a given supersaturation. In addition, the *ex situ* AFM data also show that, for Burgers vectors in excess of one-unit step height, some dislocation sources may generate hollow cores, the occurrence of which is in accordance with theoretical predictions.[37−39] The dynamics of growth steps and their consequent spreading and bunching across the {110} and {11$\bar{1}$} faces were investigated *in situ* and recorded in real time. The growth on nearly the entire both faces occurred on bunched steps (macrosteps) whose terrace width and height, despite some fluctuations, tend to increase with distance from the top of the hillock regardless of σ and the respective value of T. With the applied DICM and TBIM we estimate that the increasing terrace width range is between ∼1 and 10 μm, and the corresponding range of increasing height of macrosteps between ∼0.2 and 8 μm.

We demonstrate that the PVT growth of most perfect MHB crystals takes place in the region of lower supersaturations $(0.2 < \sigma < 0.4)$ or in terms of growth temperature (383 K $\leq T \leq$ 390 K), in which the step velocities vs supersaturation show almost a linear dependence, for both faces. For $\sigma < 0.2$, the "dead" range, no detectable growth was observed by the applied techniques for either face. The undetectable growth in this region reflects changes in the nature and operation of the primary rate controlling mechanism of growth, spiral growth. It is well founded that this could be the case, when the bulk supersaturation is low, since it has been shown[29] that locally induced stress by a pre-existing dislocation outcrop leads to the local decrease of real supersaturation around the center of the spiral. As a consequence, some of the pre-existing dislocation outcrops on a crystal seed may operate in a low mode step generation accompanied by the local deceleration of growth steps advancement at their vicinities, while the others remain inactive until the radius of curvature of the growth spiral generated by the dislocation exceeds a critical radius;[29] then growth recovers.

To get a deeper insight into the growth behavior of the {110} and {11$\bar{1}$} faces in this "dead" supersaturation region, *in situ* AFM is required.

The experimental data of step velocity vs σ and the definition of velocity, $v = \omega\beta(C_0(T_0) - C(T))$, allowed activation energies (E_{aS} and E_{aF}) and the corresponding kinetic coefficients (β_{aS} and β_{aF}) for both faces to be calculated; $E_{aS}^{(110)} \approx 30$ kJ mol^{-1}, $E_{aF}^{(110)} \approx 20$ kJ mol^{-1}, $\beta_S^{(110)} \approx 1.4 \times 10^{-6}$ cm s^{-1}, $\beta_F^{(110)} \approx 4.7 \times 10^{-4}$ cm s^{-1}, and $E_{aS}^{(11\bar{1})} \approx 50$ kJ mol^{-1}, $E_{aF}^{(11\bar{1})} \approx 33$ kJ mol^{-1}, $\beta_S^{(11\bar{1})} \approx 1.1 \times 10^{-7}$ cm s^{-1}, $\beta_F^{(11\bar{1})} \approx 3.1 \times 10^{-4}$ cm s^{-1}.

The kinetic studies now add some precision to the growth behavior of this material under ideal well-defined external conditions of temperature and supersaturation which yield crystals of high perfection. Apart from that, these studies also highlight other important issues that need to be resolved. For example, genesis of structural defects, in particular, dislocations, and the initial bunching (formation of macrosteps) even at very low supersaturations, just to mention two of them, among numerous surface processes and bulk transport phenomena taking place simultaneously, are all poorly understood. The stochastic nature of the onset of the defects,

https://doi.org/10.1021/acs.cgd.3c00097
Cryst. Growth Des. XXXX, XXX, XXX−XXX

additionally complicated by its multiparametrical character, makes the understanding of the creation of defects a huge scientific challenge. As a consequence, the prediction of conditions for growing perfect, preferably dislocation free MHB single crystals, remains open to question. Regarding step bunching, it is an intrinsic surface morphological instability not only of the {110} and {11$\bar{1}$} faces of MHB but also of any stepped face of a crystal growing either from vapor or solution phase. It is a source of structural inhomogeneities in faceted crystals and as such has a rather detrimental impact on their physical properties. As far as we are aware, the step bunching has not yet been fully rationalized and eliminated by the adjustment of external growth conditions.

Better understanding of the fundamentals of bunching phenomenon and making use of a recent rational fluid mechanics design patterns of a crystallizing media[51,52] could be a good starting point for controlling structural and compositional uniformity during crystallization not only of MHB crystals but of a wide range of nonlinear optical crystals growing from vapor phase.

Last but not least, we still do not have an answer to the question: "Why the crystals fail to grow in in a positive polar direction?" As experimentalists, in order to be able to control the crystal perfection as a whole, we need to understand a mechanistic set of events that molecules passing through, from the bulk vapor phase to their docking sites at the faces which show little or no growth in this direction. So far, this riddle has not yet been solved.

Despite the indicated challenges, our kinetic data define well the supersaturation range in which seeded crystals should grow in the most perfect state and explain the discrepancy found in our earlier attempt to use the modified Catano and Kun technique[53] to prepare and to control the preparation of larger crystals of the title material. Regrettably the present authors were unable to take the experiments to this next stage and grow large crystals at the defined growth supersaturation range of $\sigma = 0.2-0.4$ but have little doubt that similar experiments to produce large crystals in the defined supersaturation regime would be successful.

■ ASSOCIATED CONTENT

Supporting Information

The Supporting Information is available free of charge at https://pubs.acs.org/doi/10.1021/acs.cgd.3c00097.

SVP for MHB and supersaturation estimate from it (PDF)

Video of the growth of spiral growth systems (MP4)

■ AUTHOR INFORMATION

Corresponding Author

Radoljub I. Ristic − *Department of Chemical and Biological Engineering, University of Sheffield, Sheffield S1 3JD England, United Kingdom*; Email: r.i.ristic@sheffield.ac.uk

Authors

Wenbo B. Hou − *WESTCHEM, Department of Pure and Applied Chemistry, University of Strathclyde, Glasgow G1 1XL Scotland, United Kingdom;* Present Address: Wenbo Hou, St Jude Medical Center, 15900 Valley View Court, Sylmar, CA 91342, USA. wenbo11@yahoo.com

John N. Sherwood − *WESTCHEM, Department of Pure and Applied Chemistry, University of Strathclyde, Glasgow G1 1XL Scotland, United Kingdom;* orcid.org/0000-0003-3078-0928

Ranko M. Vrcelj − *WESTCHEM, Department of Pure and Applied Chemistry, University of Strathclyde, Glasgow G1 1XL Scotland, United Kingdom;* Present Address: Ranko M. Vrcelj, Centre for Defense Chemistry, Cranfield University, Defense Academy of the UK, Shrivenham, SN6 8LA, UK. ranko.vrcelj@cranfield.ac.uk.; orcid.org/0000-0001-6327-2300

Complete contact information is available at: https://pubs.acs.org/10.1021/acs.cgd.3c00097

Author Contributions

The manuscript was written through contributions of all authors. All authors have given approval to the final version of the manuscript and contributed equally.

Notes

The authors declare no competing financial interest.

■ ACKNOWLEDGMENTS

Wenbo Hou wishes to express his grateful thanks to the University of Strathclyde for the award to him of a CVCP research grant to allow him to carry out this research. The UK EPSRC is thanked for the provision of facilities provided by their general financial support of the Strathclyde laboratories. RIR and RMV would especially like to thank their colleague and friend, the late Professor John N. Sherwood, without whom this project would never have been possible. We hope we did you proud.

■ REFERENCES

(1) Chemla, D. S.; Zyss, J., Eds. *Non-Linear Optical Properties of Organic Molecules and Crystals*; Academic Press, Orlando, FL; Vol I and II, 1987.

(2) Wells, A. F. Crystal Habit and Internal Structure − I. *Philos. Mag.* **1946**, *37*, 184−199.

(3) Wells, A. F. Crystal Habit and Internal Structure − II. *Philos. Mag.* **1946**, *37*, 217−236.

(4) Wells, A. F. Abnormal and Modified Crystal Growth. *Discuss. Faraday Soc.* **1949**, *5*, 197−291.

(5) Karpinska, J.; Erxleben, A.; Mc Ardle, P. Applications of Low Temperature Gradient Sublimation in Vacuo: Rapid production of High-Quality Crystals. The first Solvent-free crystals of Ethinyl Estradiol. *Cryst.Growth Des.* **2013**, *13*, 1122−1130.

(6) Faktor, M. M.; Garrett, I., Eds. *The Growth of Crystals from the Vapour*; Chapman and Hall: London, 1974.

(7) Graska, K. Bulk Vapour Growth of CdTe. *J. Cryst. Growth* **1995**, *146*, 65−68.

(8) Singh, N.B.; Hopkins, R.H.; Mazelsky, R.; Conroy, J.J. Purification and Growth of Mercurous Chloride Single Crystals. *J. Cryst. Growth* **1986**, *75*, 173−179.

(9) Volmer, M.; Schultze, M. Kondensation und Kristallen. *Z. Physikalische Chem.* **1931**, *156A*, 1−22.

(10) Bradley, R. S.; Drury, T. The Rate of Growth of Crystals of Carbon Tetrabromide and Iodine. *Trans Farad. Soc.* **1959**, *55*, 1848−1856.

(11) Honigman, B. Züchtung größerer Einkristalle von Hexamethylentetramin aus der Dampfphase. *Z. Electrochem.* **1954**, *58*, 322−327.

(12) Honigman, B.; Heyer, H. Measurement of the Growth Mechanism of a Hexamethylenetetramine Crystal. *Z. Kristallogr.* **1954**, *106*, 199−212.

(13) Lubetkin, S. D.; Dunning, W. J. The Variability of the Rate of Growth of Adamantane Crystals from the Vapour Under Constant Conditions. *J. Cryst. Growth* **1978**, *43*, 77−80.

(14) Lubetkin, S. D.; Dunning, W. J. The Kinetics of Growth of Adamantane Crystals from the Vapour I and II. *J. Cryst. Growth* **1984**, *67*, 521−527.
(15) Morgan, A. E.; Dunning, W. J. The Growth of Monoclinic Carbon Tetrabromide Crystals. *J. Cryst. Growth* **1970**, *7*, 179−195.
(16) Sloan, G. J. Kinetics of the Crystallisation of Anthracene from the Vapor. *Mol. Cryst.* **1967**, *2*, 323−331.
(17) Karl, N. Organic Semiconductors: Purification and single crystal Growth. *Mol. Cryst.* **1989**, *171*, 157−177.
(18) McArdle, B. J.; Sherwood, J. N. Growing Organic Crystals, in *Advanced Crystal Growth*, Dryburgh, P. M.; Cockayne, B.; Barraclough, K., Eds.; Prentice-Hall: London, 1987; pp 179−217.
(19) Feigelson, R. S.; Route, R. K.; Kao, T.-M. Growth of Urea Crystals by Physical Vapour Transport. *J. Cryst. Growth* **1985**, *72*, 585−594.
(20) Zha, M.; Franzosi, P.; Zanotti, L.; Zuccalli, G.; Paorici, C.; Capelletti, R. Growth and Characterisation of Urea Crystals by Physical Vapour Transport in Semi-open Cells. *J. Cryst. Growth* **1995**, *146*, 29−36.
(21) Hou, W.; Ristic, R. I.; Hammond, R. B.; Vrcelj, R. M.; Sheen, D. B.; Sherwood, J. N. Crystal Growth of the Acentric Organic Non-Linear Optical Material Methyl-p-Hydroxybenzoate (MHB): Morphological Variations in Crystals Grown by Physical Vapour Transport. *Cryst. Growth Des.* **2019**, *19*, 5505−5515.
(22) Hou, W.; Ristic, R. I.; Sherwood, J. N.; Vrcelj, R. M. Seeded Crystal Growth of the Acentric Organic Nonlinear Optical Material Methyl-p-Hydroxybenzoate from the Vapor Phase. This Paper.
(23) Hou, W.; Ristic, R. I.; Sherwood, J. N.; Vrcelj, R. M. Crystal Growth of the Acentric Organic Non-Linear Optical Material Methyl-p-Hydroxybenzoate (MHB): Comparison of Growth from the Vapour Phase and from Solutions. In Preparation.
(24) Jerphagnon, J. Optical Second Harmonic Generation in Isocyclic and Heterocyclic Compounds. *IEEE J. Quantum Electron.* **1971**, *7*, 42−43.
(25) Srinivasan, K.; Sherwood, J. N. Asymmetric Growth of Alpha-Resorcinol Crystals: Comparison of growth from the vapour phase and from solution. *Cryst. Growth Des.* **2005**, *5*, 1359−1370.
(26) Perlovich, G. L.; Radionov, S. L.; Bauer-Brandl, A. Thermodynamics of Solubility, Sublimation and Solvation Processes of Parabens. *Eur. J. Pharm. Sci.* **2005**, *24*, 25−33.
(27) Liu, Y.; Black, J. F. B.; Boon, K. F.; Cruz-Cabeza, A. J.; Davey, R. J.; Dowling, R. J.; George, N.; Hutchinson, A.; Montis, R. When Crystals Do Not Grow: The Growth Dead Zone. *Cryst. Growth and Design* **2019**, *19*, 4579−4587.
(28) Threlfall, T. L.; Coles, S. J. A perspective on the growth-only zone, the secondary nucleation threshold and crystal size distribution in solution crystallisation. *CrystEngComm.* **2016**, *18*, 369−378.
(29) Chernov, A. A. Formation of Crystals in Solution. *Contemporary Physics.* **1989**, *30*, 251−276.
(30) Compton, R. G.; Unwin, P. R. The dissolution of calcite in aqueous solution at pH < 4: Kinetics and mechanism. *Philos. Trans. R. Soc. London A* **1990**, *330*, 1−45.
(31) Knippenberg, W. F. Thesis. *Philips Res. Rept.* **1963**, *18*, 161.
(32) Sunagawa, I.; Bennema, P. Observation of the influence of stress fields on the shape of growth and dissolution spirals. *J. Cryst. Growth* **1981**, *53*, 490−504.
(33) Amelinckx, S.; Strumane, G. Silicon Carbide; A High Temperature Semiconductor. In *Proceedings from Conference on Silicon Carbide*, Pergamon: Boston, 1959; p 162.
(34) Verma, A. R. *Crystal Growth and Dislocations*; Butterworths: London, 1953.
(35) De Yoreo, J. J.; Land, T. A.; Lee, J. D. Limits on Surface Vicinality and Growth Rate due to Hollow Dislocation Cores on KDP {101}. *Phys. Rev. Lett.* **1997**, *78*, 4462−4465.
(36) Qian, W.; Rohrer, G. S.; Skowronski, M.; Doverspike, K.; Rowland, L. B.; Gaskill, D. K. Open-core screw dislocations in GaN epilayers observed by scanning force microscopy and high-resolution transmission electron microscopy. *Appl. Phys. Lett.* **1995**, *67*, 2284−2286.
(37) Frank, F. C. Capillary equilibria of dislocated crystals. *Acta Crystallogr.* **1951**, *4*, 497−501.
(38) Cabrera, N.; Levine, M. M. On the dislocation theory of evaporation of crystals. *Philos. Mag.* **1956**, *1*, 450−458.
(39) Van der Hoek, B.; van der Eerden, J. P.; Bennema, P. Thermodynamical Stability Conditions for the Occurrence of Hollow Cores Caused by Stress of Line and Planar Defects. *J. Cryst. Growth* **1982**, *56*, 621−623.
(40) Bauser, E. Atomic mechanisms in semiconductor liquid phase epitaxy. In *Handbook of Crystal Growth*, Hurle, D. T. J., Ed.; North Holland: Amsterdam, 1994; pp 879−911.
(41) Sato, M.; Uwaha, M.; Saito, Y. Instabilities of steps induced by the drift of adatoms and effect of the step permeability. *Phys. Rev. B* **2000**, *62*, 8452−8472.
(42) Fujita, K.; Ichikawa, M.; Stoyanov, S. S. Size-scaling exponents of current-induced step bunching on silicon surfaces. *Phys. Rev. B* **1999**, *60*, 16006−16012.
(43) Golightly, J. P. Hollow screw dislocation cores in silicon carbide. *Z. Kristallogr.* **1969**, *130*, 310−313.
(44) Sunagawa, I. *Crystals Growth, Morphology, and Perfection*; Cambridge University Press, 2005.
(45) Van Enckevort, W. J. P. Growth Steps on Crystal Surfaces: Their observation and interpretation. *Current Topics in Crystal Growth Research* **1995**, *2*, 535−551.
(46) Van den Berg, E. P. G.; Sweegers, A. J. R.; Verheijen, M. A.; van Enckevort, W. J. P. In Situ Topography of the (200) face of ϵ Caprolactam Growing from the Vapour Phase. *J. Cryst. Growth* **1997**, *180*, 284−292.
(47) Burton, W. K.; Cabrera, N.; Frank, F. C. The growth of crystals and the equilibrium structure of their surfaces. *Philos. Trans. R. Soc. London A* **1951**, *243*, 299−358.
(48) Chernov, A. A. *Modern Crystallography III. Crystal Growth*; Springer: Berlin and New York, 1984; Vol. *36*.
(49) Malkin, A. J.; Land, T. A.; Kuznetsov, Yu. G.; McPherson, A.; De Yoreo, J. J. Investigation of Virus Crystal Growth Mechanisms by In Situ Atomic Force Microscopy. *Phys. Rev. Lett.* **1995**, *75*, 2778−2781.
(50) Malkin, A. J.; Land, T. A.; Kuznetsov, Yu. G.; McPherson, A.; De Yoreo, J. J. Mechanisms of Protein Crystal Growth: An Atomic Force Microscopy Study of Canavalin Crystallization. *Phys. Rev. Lett.* **1995**, *75*, 2774−2777.
(51) Booth, N. A.; Chernov, A. A.; Vekilov, P. G. Characteristic length-scales of step bunching in KDP crystal growth: in situ differential phase-shifting interferometry study. *J. Cryst. Growth.* **2002**, *237-239*, 1818.
(52) Ristic, R. I. Oscillatory Mixing for Crystallization of High Crystal Perfection Pharmaceuticals. *Chemical Engineering Research & Design.* **2007**, *85*, 937−944.
(53) Catano, A.; Kun, Z. K. Growth and Charaterisation of ZnSe and Homogeneous ZnSxSe-x Crystals. *J. Cryst. Growth* **1976**, *33*, 324−330.

https://doi.org/10.1021/acs.cgd.3c00097
Cryst. Growth Des. XXXX, XXX, XXX−XXX